journal

J. Am. Ceram. Soc., 1–11 (2012)
DOI: 10.1111/jace.12120

Effects of Tm^{3+} Additions on the Crystallization of LaF_3 Nanocrystals in Oxyfluoride Glasses: Optical Characterization and Up-Conversion

A.de Pablos-Martín,[‡,§,†] D. Ristic,[¶] S.Bhattacharyya,[‖,††] Th. Höche,[§,‖] G.C. Mather,[‡] M.O Ramírez,[‡‡] S. Soria,[§§] M. Ferrari,[¶] G.C. Righini,[§§] L.E. Bausá,[‡‡] A. Durán,[‡] and M.J. Pascual[‡]

[‡]Instituto de Cerámica y Vidrio (CSIC), C/Kelsen 5, Campus de Cantoblanco, 28049 Madrid, Spain

[§]Fraunhofer Institute for Mechanics of Materials IWM, Walter-Hülse-Str. 1, D-06120 Halle, Germany

[¶]CNR-IFN, CSMFO Group, Istituto di Fotonica e Nanotecnologie, via alla Cascata 56/C, 38050 Povo, Italy

[‖]Leibniz-Institut für Oberflächenmodifizierung e.V., Permoserstraβe 15, D-04318 Leipzig, Germany

[††]Department of Condensed Matter Physics and Materials Science, Tata Institute of Fundamental Research, Mumbai 400005, India

[‡‡]Departamento de Física de Materiales, Universidad Autónoma de Madrid, 28049 Madrid, Spain

[§§]MDF Lab (Photonic Materials and Devices), CNR – Nello Carrara Institute of Applied Physics, via Madonna del Piano 10, 50019 Sesto Fiorentino, Firenze, Italy

The influence of the addition of 1 mol% Tm_2O_3 on the nano-crystallization of LaF_3 in a glass of composition $55SiO_2$–$20Al_2O_3$–$15Na_2O$–$10LaF_3$ (mol%) has been studied. Tm_2O_3 affects the phase separation in the glass and delays the onset of crystallization with respect to the undoped glass. Additionally, the maximum LaF_3 crystal size is slightly greater than that in the undoped glass–ceramics. The microstructural and compositional changes in the glass matrix have been studied using several techniques, including viscosity, dilatometry, X-ray and neutron diffraction (XRD, ND), quantitative Rietveld refinement, transmission electron microscopy (TEM), differential scanning calorimetry (DSC), and Raman spectroscopy. Photoluminescence measurements indicate that the Tm^{3+} ions are distributed between the glassy matrix and LaF_3 crystals. Eu_2O_3 has been used as structure probe and part of the Eu^{3+} ions are reduced to Eu^{2+} when incorporated in the LaF_3 nano-crystals. Up-conversion spectra under IR-excitation show a higher intensity of the blue emission in the Tm-doped glass–ceramic compared with that in the glass.

I. Introduction

Oxyfluoride glass–ceramics containing nano-crystals have been extensively researched since Wang and Ohwaki[1] developed Yb^{3+}/Er^{3+}-doped $Pb_xCd_{2-x}F_2$ nanocrystals within an oxide glassy matrix. Investigations have involved adding different dopant ions and exploring new crystalline phases, such as CaF_2,[2,3] PbF_2[4–6] and LaF_3.[7–10] This last phase is one of the most commonly selected fluorides for hosting rare-earth (RE) ions, as it has the second lowest phonon energy of the commonly used RE-doped matrices. Moreover, the similarity of the La^{3+} atomic radius to those of RE cations allows its substitution with very little change in the crystal structure.

Studies of RE-doped materials are mainly focused on optical properties, with the crystallization mechanisms less well understood. Only a few investigations have analyzed the effect of the addition of RE ions on crystallization. Chen *et al.*[8] reported a glass composition in the SiO_2–Al_2O_3–NaO_2–LaF_3 system doped with Yb^{3+}, in which the RE cation acts as a nucleation agent for a diffusion-controlled crystallization mechanism. Hu *et al.*[11] reported the nucleating effect of Er^{3+} ions in the same glass and the higher quantity and smaller size of LaF_3 crystallites after heat treatment compared with the undoped composition. Barros *et al.*[12] documented that the addition of Er^{3+} and Sm^{3+} to the SiO_2–Al_2O_3–NaO_2–BaF_2 system, in which crystallization of cubic BaF_2 occurs, favors phase separation, which is not observed in the undoped material. The BaF_2 crystals are formed within the phase-separated droplets, which are likely to hinder diffusion and affect the overall crystallization process; however, there was no evidence provided for the location of Er^{3+} and Sm^{3+} in the crystalline phase.

We previously reported nano-crystallization of LaF_3 in a glass of composition 55 SiO_2–20 Al_2O_3–15 Na_2O–10LaF_3 (mol%). The parent glass is phase separated and contains La-enriched droplets. The crystallization, which takes place on thermal treatment, involves a variation in the chemical composition in the glass matrix and an increase in viscosity. The formation of a crystal-glass interface enriched in SiO_2 takes place, which acts as a diffusion barrier leading to a variation in the crystal-growth velocity.[13–15]

The present study focuses on the effects of dopant Tm^{3+} ions on LaF_3 crystallization in the same glass composition. The Tm^{3+} ion is studied in more detail because of its blue up-conversion emission occurring on excitation at 790 nm, which has potential application in optical devices for high optical-density storage,[16] under-sea optical communications and, in the field of medicine, for biomedical diagnostics.[17] Nevertheless, Tm^{3+}-doped materials are generally difficult to analyze as the energy levels of Tm^{3+} ions are highly symmetrical and very sensitive to concentration quenching. Eu^{3+} may be used as a structural probe because it shows a single exponential decay[18] and does not exhibit quenching at concentrations as high as 3 mol%. Hence, glass–ceramics doped with Eu^{3+} were also prepared to study the distribution of the RE ions between the glass matrix and crystals. Optical characterization of the Tm^{3+}- and Eu^{3+}-doped glasses and glass–ceramics involving absorbance and

J. McKittrick—contributing editor

Manuscript No. 31562. Received June 4, 2012; approved November 5, 2012.
†Author to whom correspondence should be addressed. e-mail: araceli.pablos@icv.csic.es

emission spectroscopy, including up-conversion emission and luminescence-decay curve analysis, has also been undertaken.

II. Experimental Procedure

(1) Glass Melting and Chemical Analysis

Two glasses of nominal composition $55SiO_2$–$20Al_2O_3$–$15Na_2O$–$10LaF_3$ (mol%) doped with either 1 mol% of Tm_2O_3 or 0.5 mol% Eu_2O_3 were prepared by melting reagent-grade SiO_2 (99.6%; Saint Gobain, Aviles, Spain), Al_2O_3 (Panreac), Na_2CO_3 (99.5%; Panreac, Barcelona, Spain), LaF_3 (99%; Panreac), Tm_2O_3 (99.9%; GFS Chemicals GFS Chemicals Inc., Powell, Ohio) and Eu_2O_3 (99.995%; Inframat Advanced Materials, Manchester, Connecticut) in an electric furnace. The batches were first calcined for 2 h at 1200°C and then melted at 1600°C for 1.5 h. The melts were quenched twice in air onto a brass mold to obtain homogeneous transparent glasses, which were then annealed at T_g + 5°C for 30 min. The glass composition was analyzed using X-ray fluorescence spectroscopy with a Panalytical spectrometer. The content of all oxides was determined using the melting method with $Li_2B_4O_7$; the fluorine content was analyzed employing pressed pellets of powdered glass (8 g) to avoid volatilization.

Glass–ceramics were obtained after heat treatments at 620°C from 10 to 80 h; this procedure is the same as that used previously for the undoped glass.[15]

(2) Dilatometry and Differential Scanning Calorimetry

The glass-transition temperature (T_g) was determined by dilatometry in a Netzsch dilatometer, model 402 EP, using a heating rate of 10 K/min in air (estimated error of T_g is ±2°C).

DSC measurements were performed using a Setaram instrument (Model Setsys Evolution 16/18, Setaram, Cambridge, UK) using powdered Al_2O_3 as inert reference material and employing 100–150 mg of glass with particle size of 1–1.25 mm to reproduce bulk conditions. The DSC scans were carried out with heating rates in the range 5–30 K/min to determine the activation energy for crystallization, the Avrami parameter, and the dimensionality of crystal growth.

(3) X-ray and Neutron Diffraction

The glass–ceramics were characterized by powder XRD employing a D5000 Siemens diffractometer (Siemens AG, Munich, Germany) with monochromatic Cu$K\alpha$ radiation (1.5418 Å). Patterns were scanned over the angular range $20 \leq 2\theta \leq 60°$ with a step size of 0.05° and a fixed counting time of 2.5 s per step.

The crystallized fraction of LaF_3 of the glass–ceramics obtained at 620°C during 40 h was estimated by quantitative Rietveld analysis of XRD data, employing a similar method to that applied previously for the undoped composition.[15] The glass was ground to a fine powder in an agate mortar, sieved through a 60 μm mesh then milled again with NaF (99.9%; PRO-VYS, Prague, Czech Republic), which was used as internal standard in a suitable quantity (3 wt%) to approximate the peak intensity of the crystalline LaF_3. The average particle size of the NaF internal standard was determined to be 11.4 μm using the laser light dispersion method with a Mastersizer S instrument (Malver Instruments Ltd., Malvern, UK). XRD powder data for Rietveld analysis were collected over the range $10° \leq 2\theta \leq 110°$ in a stepwidth of 0.0197° and a fixed counting time of 620 s employing an X'Pert PRO Panalytical diffractometer (PANalytical, Almelo, The Netherlands) equipped with an X'Celerator detector and monochromatic Cu$K\alpha$ radiation. Rietveld refinement was carried out with the FULLPROF program[19] using interpolation of background points to model the amorphous contribution to the pattern.

In situ neutron-diffraction measurements were performed on the D1B diffractometer (ILL, Grenoble, France) in the range $16 \leq 2\theta \leq 96°$, using the λ = 2.52 Å line. The glasses were cut in square-sectioned bars (diameter, 7–7.5 mm; length 10–50 mm) and placed in a vanadium tube sample holder located in a vacuum furnace. Heating of the sample started once the vacuum reached a pressure of 10^{-1} mbar. The heating ramp and neutron flux were programmed in the following sequence: (1) from room temperature to 550°C without neutron flux; (2) from 550°C to 620°C, with the neutron beam activated during which time a diffractogram was recorded every 2 min; (3) a dwell of 8.5 h at 620°C for 8.5 h during which diffractograms were also recorded every 2 min.

(4) Transmission Electron Microscopy

Oxyfluoride glass and glass–ceramic samples for TEM were prepared by cutting slices, plane-parallel grinding, dimpling to a residual thickness of 10–15 μm, and ion-beam thinning using Ar^+ ions. To avoid substantial heating of the TEM foils and, hence, the introduction of artifacts, double-sided ion-beam etching was performed at small angles (5°) and a low ion-beam energy (acceleration voltage, 2.5 kV; beam current, <9 μA). The non-conducting samples were selectively coated with carbon[20] prior to investigation to reduce charging effects under the electron beam. The samples were then characterized with a Hitachi H-8100 transmission electron microscope (Hitachi High Technologies Corp., Tokyo, Japan) equipped with a LaB_6 filament operating at an acceleration voltage of 75 kV.

(5) Viscosity

The glass viscosity was determined by the rotation method in the range 10^3–10^1 dPa s employing a high-temperature Haake viscometer (Haake, Karlsruhe, Germany) equipped with a ME 1700 sensor. Rotation speeds of 1–30 rpm were used for 10 min and the International Standard ISO 7884-2 was followed. Three measurements were carried out at three different rotation speeds for each temperature.

Hot stage microscopy (HSM) was performed in a Leica-EM201 microscope (Leica Microsystems GmbH, Wetzlar, Germany) with image analysis for determination of the viscosity in air at a heating rate of 5 K min^{-1}. The samples were initially cold pressed to conformed bodies of 3 mm in both height and diameter from glass powder with a particle size <60 μm. The temperature was measured with a Pt/Rh (6130) thermocouple placed under and in contact with the alumina support. The temperatures corresponding to the characteristic viscosity points, following Scholze's definition,[21,22] were obtained from photomicrographs.

The viscosity–temperature curve was obtained by combining the experimental data from the rotation method, HSM and the T_g from the DSC curve obtained at a rate of 10 K/min.

(6) Optical Spectroscopy

Raman scattering of the Tm-doped glass and glass–ceramics was measured at room temperature in the wave-number range, 100–1000 cm^{-1}. A microprobe setup (Horiba-Jobin-Yvon; LabRam Aramis, HORIBA Ltd., Kyoto, Japan) consisting of a diode laser operating at 532 nm, a narrowband notch filter, a 46 cm focal length spectrograph using a 1200 grooves/mm grating, and a charge-coupled device detector was employed. Exciting radiation (532 nm) was focused onto the sample surface with a spot size of 1 μm^2 through a 100X objective with numerical aperture of 0.9; the resolution was 0.35 cm^{-1}/pixel. Absorbance spectra were recorded at room temperature using a Perkin Elmer Lambda 950 spectrometer in the range 300–880 nm.

Photoluminescence of the Tm^{3+} and Eu^{3+} ions was performed at room temperature under excitation with an Argon laser tuned at 488 nm. The laser beam was focused onto the sample by a microscope objective lens. The photolumines-

cence was collected in backscattering geometry with the same objective lens and focused into a multimode fiber. The end of the fiber was directly connected to the spectrometer and the signal was detected with a Peltier-cooled, charge-coupled device camera. A beam splitter and notch filter were used to attenuate the pump laser line. The spectral resolution was about 0.1 nm. Additionally, Eu^{3+} photoluminescence spectra were collected at an excitation of 393 nm.

Up-conversion emission spectra were collected at room temperature under excitation with a Ti: sapphire pulsed laser at 790 nm. A Multiphoton Microscope was used, consisting of a Nikon PCM2000 (Nikon Instruments, Tokyo, Japan) confocal laser scanning microscope, equipped with a Nikon TE2000-U inverted optical microscope. The laser source is directly coupled to the confocal scanning unit, after first transversing a Faraday isolator (to avoid the part of the laser beam that can return to the laser cavity).

III. Results and Discussion

(1) Study of LaF_3 Crystallization in 1 mol% Tm_2O_3-Doped Glasses

Table I lists the theoretical and analyzed compositions of both undoped and 1 mol% Tm_2O_3 -doped glasses. Fluorine loss during the melting process, calculated by chemical analysis, corresponds to 38 and 27 wt% in the undoped glass and Tm_2O_3-doped glasses, respectively. As reported by Sroda,[23] RE ions, Tm in this case, play a similar role to aluminum, but their effective radii are more than double that of Al^{3+} such that the RE ions form weaker oxygen bonds. Thus, it appears that the Al ions bond preferentially with oxygen ions, while Tm ions may contribute to the retention of fluorine ions.

Dilatometry indicates that the glass-transition temperature, T_g, of the 1 mol% Tm_2O_3-doped glass is 622°C, which is 24°C higher than that of the undoped glass reported previously.[15] Sroda[23] also reported an increase in the T_g up to 25°C with the addition of 1 mol% Er_2O_3 in a glass of composition $67SiO_2$–$9Al_2O_3$–$20Na_2O$–Al_2F_6–$3La_2F_6$ mol%, attributing the rise to the additional O^{2-} ions, which increase the polymerization of the network. The higher T_g in the Tm-doped glass can also be attributed to differences in phase separation already present in the parent glasses, as will be further detailed below.

(A) X-ray and Neutron Diffraction: Figure 1(a) shows the XRD patterns of 1 mol% Tm_2O_3–doped glass–ceramics obtained from isotherms of 10–80 h at 620°C, which correspond to that of hexagonal LaF_3 (JCPDS 32-0483). The first diffraction peaks are observed after 10 h of treatment (Fig. 1), and become increasingly sharper and more intense with time of treatment, concomitant with the increase in crystalline fraction.

XRD lines were fitted by a Gaussian profile shape function and the size of the crystals was calculated using the Scherrer Eq. (1) on the $2\theta \approx 27.5°$ peak of LaF_3 (111):

$$D = \frac{G\lambda}{B\cos\theta} \quad (1)$$

where D is the crystal size, G is a constant whose value is 0.9, B is the corrected full width at half maximum of the peak and θ is the Bragg angle. Figure 1(b) reveals the calculated crystal sizes corresponding to Fig. 1(a). The crystal sizes of the undoped glass–ceramics reported in ref. [15] are also shown for comparison. In the undoped glass–ceramics, LaF_3 diffraction peaks appear after 1 h of treatment at 620°C and the crystal size increases rapidly until a maximum of 9 nm is reached.[15] In contrast, a significant initial growth of the crystals in the Tm^{3+}-doped glass–ceramics is not observed, as diffraction peaks are only detectable after 10 h of treatment. From 20 h onward, the crystal size remains constant with time at a maximum size of 19 nm, higher than that of the undoped glass–ceramics. Hu *et al.*[11] also obtained greater crystals sizes in RE-doped glass–ceramics with respect to the undoped analogues, explaining that the effective

Table I. Nominal and Analyzed Compositions in wt% of the Undoped and Tm-Doped Glasses

	Undoped glass ref. [15]		1 mol% Tm_2O_3-doped glass	
Component	Theoretical (wt%)	Analyzed (wt%)	Theoretical (wt%)	Analyzed (wt%)
SiO_2	40.1	38.7 ± 0.3	38.34	38.0 ± 0.3
Al_2O_3	24.8	24.3 ± 0.1	23.66	22.5 ± 0.1
Na_2O	11.3	10.7 ± 0.4	10.79	10.2 ± 0.4
LaF_3	23.8	14.7	22.72	16.6
La_2O_3		22.9 ± 0.1		21.7 ± 0.1
Tm_2O_3	–	–	4.47	3.65 ± 0.10
F	6.90	4.30 ± 0.15	6.61	4.84 ± 0.15
F Loss%	38		27	

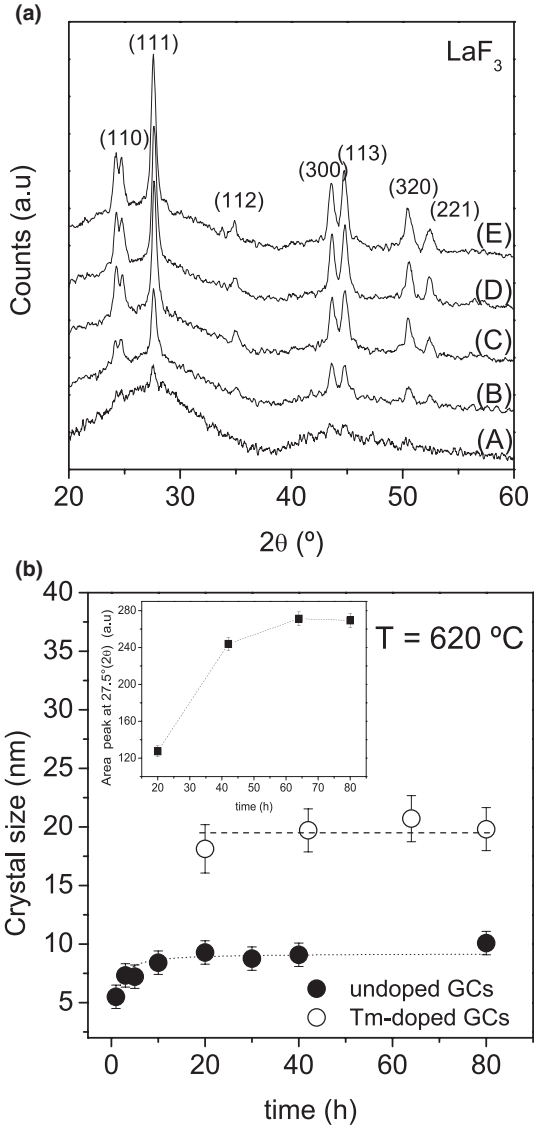

Fig. 1. (a) XRD patterns of 1 mol% Tm_2O_3-doped glass obtained at 620°C during 10 h (A), 20 h (B), 42 h (C), 62 h (D), and 80 h (E). LaF_3 diffraction planes are indicated. (b) Crystal size as a function of time of treatment at 620°C of the 1 mol% Tm_2O_3-doped glass–ceramics and of the undoped glass–ceramics.[15] Time dependence of the area under the diffraction peak at $2\theta \approx 27.5°$ is shown in the inset.

concentration (or chemical activity) of RE ions in the crystallites is probably greater than that on the surface, promoting surface mobility and enhancing crystallite growth.

As a measure of the dependence of crystalline fraction with time of treatment at 620°C, the area under the diffraction peak at $2\theta \approx 27.5°$ was plotted as a function of time [inset of Fig. 1(b)]. A rapid increase in the peak area is observed from 20 to 42 h, while for longer treatment times the area increases more slowly and then stabilizes. From 20 to 42 h, the quantity of crystals increases rather than their size. Hence, it is proposed[24] that nucleation takes place in the glass–ceramic regions, in which the chemical composition presents T_g values below the treatment temperature. The nucleation process continues until the T_g of the glass–ceramics is close to the treatment temperature, after which further nucleation and crystallization are impeded. Our results thus support the hypothesis of formation of a diffusional barrier which inhibits crystal growth, as shown in the undoped glass.[15]

Structural models of LaF_3 (space group, $P\bar{3}c1$) and the NaF internal standard ($Fm\bar{3}m$) were refined by Rietveld analysis based on the reported structures.[25,26] The effects of the hexagonal shape of the LaF_3 crystals on the diffraction data were incorporated into the Rietveld refinement by means of refining preferred orientation parameters. The thermal vibration factors of the two phases were not refined to avoid correlation with the background or other parameters.[27] The observed diffraction pattern and the difference pattern between observed and calculated data on termination of Rietveld refinement are shown in Fig. 2. Final structural parameters and reliability factors indicating the quality of the refinement are listed in Table II. The refined lattice parameters of the Tm^{3+}-doped crystals are slightly shorter than those calculated for the undoped glass–ceramic,[15] more so along the c axis, which provides evidence that the Tm^{3+} substitutes to some extent the larger La^{3+} ion in the crystal lattice. Nevertheless, the occupation of the La site by Tm was not incorporated into the structural model as the resolution of the X-ray data was not sufficient to permit an accurate analysis for such a low doping content.

The weight fraction of LaF_3 obtained by refinement was corrected for the presence of the amorphous phase from the X-ray and real weight fractions of the NaF internal standard with the same procedure as outlined in previous works.[28,29] The actual weight fraction of LaF_3 in the glass, after correction for the presence of the NaF standard in the refinement data, was calculated to be 6.3 wt%, similar to the quantity calculated for the corresponding undoped glass–ceramic after an equivalent heat treatment.[15]

In situ neutron diffraction experiments were also performed (Fig. 3) to investigate the different crystallization kinetics of the Tm^{3+}-doped and undoped glasses [Fig. 1(a)]. In the undoped glass [Fig. 3(a)], the first recorded diffractogram was collected after 2 min at 620°C, after which time LaF_3 diffraction peaks can already be discerned. These peaks become better resolved with time up to 5 h of treatment. The

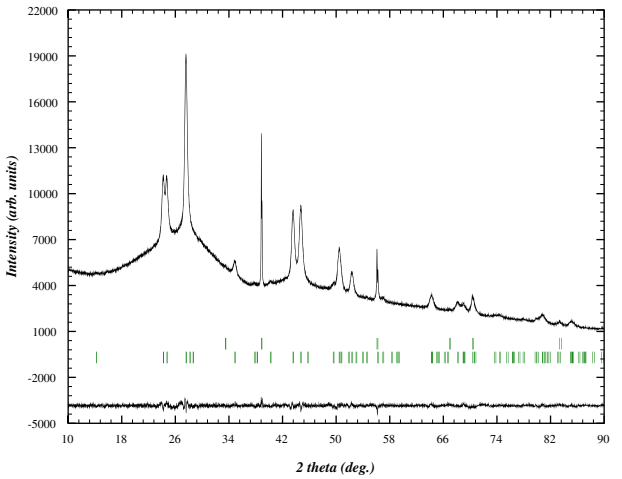

Fig. 2. Observed and difference X-ray powder diffraction files of 1 mol% Tm_2O_3-doped glass–ceramic obtained at 620°C during 40 h, with 3% NaF as internal standard. The Bragg peaks of NaF and LaF_3 are indicated by top and bottom vertical bars, respectively

Table II. Structure Refinement Data for 1 mol% Tm-Doped LaF_3 Nanocrystals. Space Group $P\bar{3}c1$; a = 7.1923(4) Å; c = 7.3517(5) Å; R_p = 1.47; R_{wp} = 1.94; χ^2 = 1.52

Atom	Site	x/a	y/b	c/z	occupancy
La(1)	6*f*	0.6777 (7)	0	1/4	1.0
F(1)	12*g*	0.344 (3)	0.065 (2)	0.0741 (8)	1.0
F(2)	4*d*	1/3	2/3	0.133 (2)	1.0
F(3)	2*a*	0	0	1/4	1.0

Thermal vibration factors were constrained to B_{iso} = 1.0

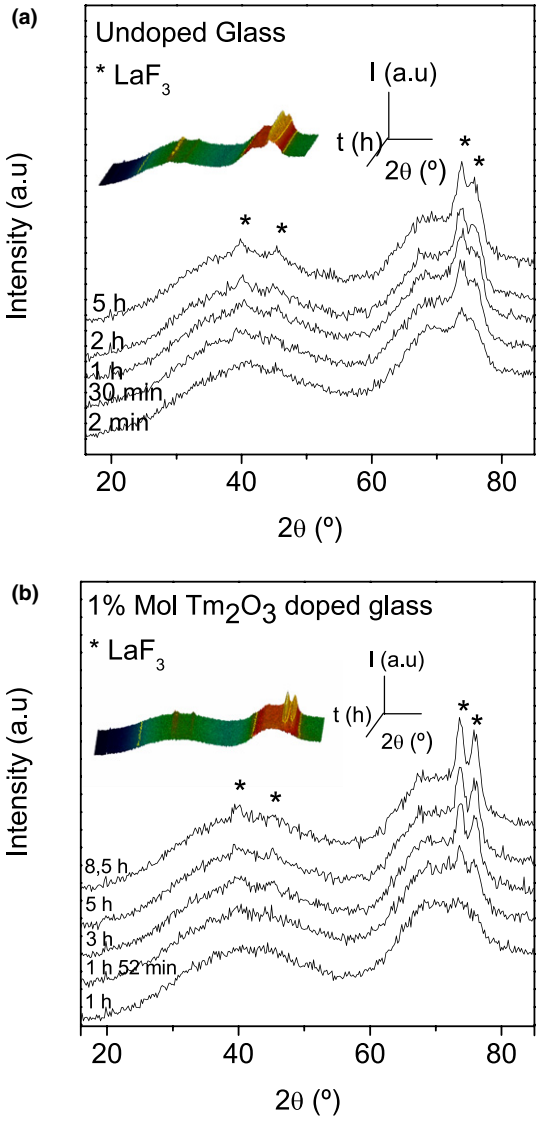

Fig. 3. In situ neutron diffraction patterns of (a) undoped glass annealed at 620°C for up to 5 h, (b) 1 mol% Tm_2O_3-doped glass annealed at 620°C for up to 8.5 h. The corresponding 3-D in situ neutron diffraction patterns are shown in the inset of each figure.

Tm^{3+}-doped glass shows the first diffraction peak after almost 2 h of treatment at 620°C [Fig. 3(b)], and the peaks increase in intensity with time. This delay in crystallization in the Tm^{3+}-doped glass with respect to the undoped glass can be observed clearly in a 3-D diffractogram plot [inset of Figs. 3(a) and (b)]. It suggests that LaF_3 crystallization occurs in the Tm-doped glass after a longer induction time with respect to the undoped glass.

(B) Transmission Electron Microscopy: Figures 4(a) and (b) show transmission electron micrographs of the undoped parent glass and glass–ceramic obtained at 620°C for 40 h, respectively.[15] The corresponding micrographs of the Tm-doped glass and glass–ceramic prepared under the same conditions are shown in panels c and d of Fig. 4.

The micrographs of both the doped and undoped parent glasses reveal phase separation involving amorphous La-enriched droplets in the range of 15–20 nm. The droplets in the Tm-doped glass seem to be somewhat larger than those of the undoped material. An enhancement of phase separation with Tm_2O_3 additions could contribute to an increase in T_g. Barros *et al.*[12] observed that the addition of RE cations affects phase-separation, although the reason for such behavior is not yet clear.

A homogenous distribution of LaF_3 nano-crystals is observed for both glass–ceramics [Figs. 4(b) and (d)]. The transmission electron micrograph of the Tm^{3+}-doped glass–ceramic [Fig. 4(d)] shows a more extended phase separation than that of the un-doped material [Fig. 4(b)], which corresponds well with the observation stated in the above paragraph. This phase separation may, in addition to crystalline LaF_3, also result in the formation of amorphous regions which do not contribute to an increased LaF_3 crystalline fraction. The slightly bigger crystal size in the Tm-doped glass–ceramic compared with the undoped glass–ceramic is in good agreement with Fig. 1(b), and favors the formation of agglomerates.

(C) Differential Scanning Calorimetry: The DSC curves of the 1 mol% Tm_2O_3-doped glass and those of the undoped glass reported in[15] at 10 K/min are shown in Fig. 5(a). The Tm_2O_3-doped glass exhibits a glass-transition temperature of 608°C, which is 18°C higher than that of the undoped glass (590°C), in good agreement with the values obtained by dilatometry. An exothermic crystallization peak is observed in the Tm_2O_3-doped glass at 752°C. Heat treatment at this temperature for 1 h leads to the crystallization of LaF_3 (XRD pattern not shown) and the sample becomes translucent.

The crystallization peak is observed at 693°C in the undoped glass, which is a much lower temperature than that of the crystallization peak in the Tm-doped glass (752°C). Hence, the increase in the fluoride crystallization temperature with the addition of Tm_2O_3 is consistent with the delayed onset of LaF_3 crystallization and with the longer induction time in the Tm-doped glass compared with the undoped glass, shown in Fig. 3.

The DSC curves of the Tm_2O_3-doped glass recorded at different heating rates, Fig. 5(b), show one crystallization peak. Table III lists the LaF_3 crystallization temperatures, T_p, for both the Tm-doped and undoped glasses,[15] and the corresponding temperatures of the onset of crystallization, T_x. The Avrami exponent, n, was derived from Avrami's law, following a previously reported procedure[15] involving Ozawa's Eq. (2):

$$\frac{d[\ln[-\ln(1-x)]]}{d[\ln Q]}\Big|_T = -n \tag{2}$$

where Q represents the heating rate and x is the ratio between the partial area of the crystallization peak at a fixed

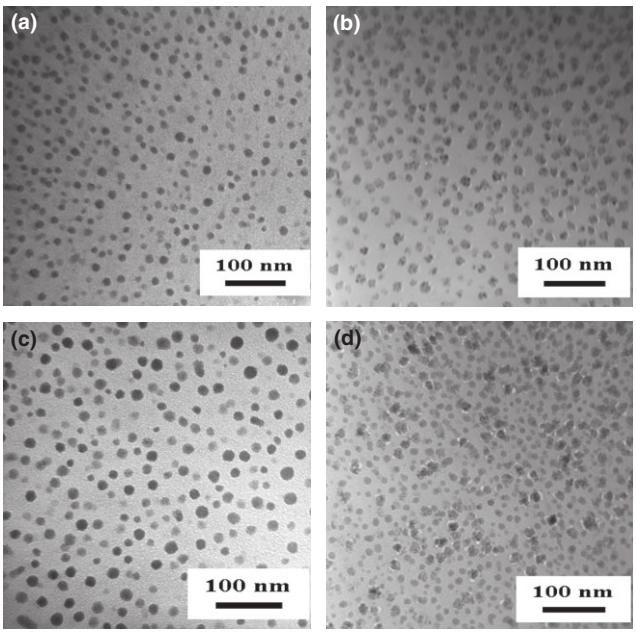

Fig. 4. Transmission electron micrographs of (a) undoped glass, (b) undoped glass–ceramic obtained at 620°C, 40 h, (c) 1 mol% Tm_2O_3-doped glass and (d) 1 mol% Tm_2O_3-doped glass–ceramic obtained after 40 h at 620°C.

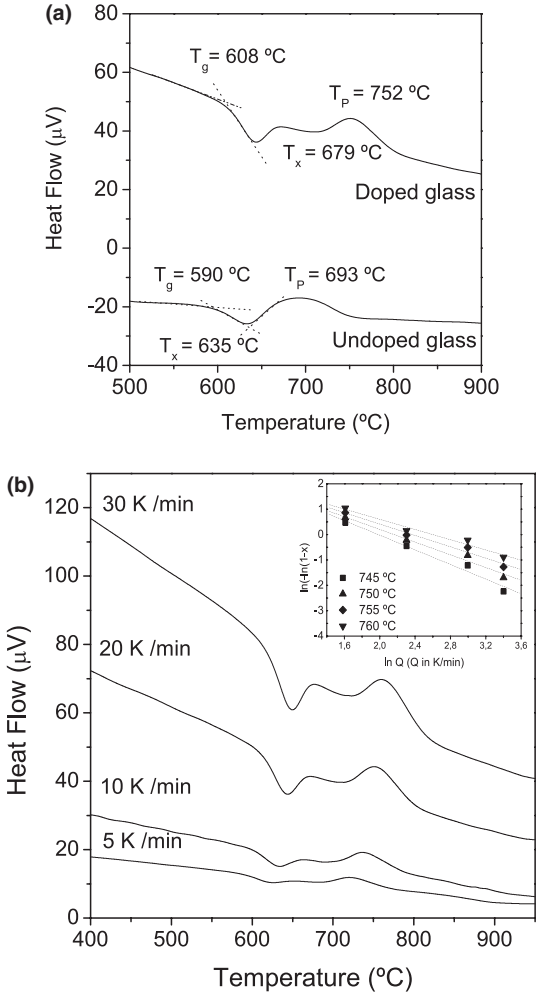

Fig. 5. (a) DSC Curves at 10 K/min of the undoped and 1 mol% Tm_2O_3-doped glass, (b) DSC curves of the 1 mol% Tm_2O_3-doped glass at different heating rates. The inset shows the Ozawa plot from 740°C to 760°C for the determination of the Avrami exponent n.

Table III. T_x and T_p Values Obtained from DSC Curves at Different Heating Rates

Q (K/min)	T_x (°C) ± 2 of undoped glass in ref. [15]	T_x (°C) ± 2 of studied doped 1 mol% Tm_2O_3 glass	T_p (°C) ± 2 of undoped glass in ref. [15]	T_p (°C) ± 2 of studied doped 1 mol% Tm_2O_3 glass
5	616	685	667	721
10	635	693	679	737
20	636	713	693	753
30	643	725	703	764

temperature and the total area of the peak.[30] The inset of Fig. 5(b) shows the Ozawa plot, from which x was calculated to be in the range 745°C–760°C. Table IV summarizes the calculated Avrami parameters, where the average value of n is 1.3, approaching a value equal to 1.

To determine the apparent activation energy for crystallization, the data obtained using different heating rates, Fig. 5(b), can be analyzed adopting two different assumptions: (i) crystal growth occurs from a fixed number of nuclei or (ii) further nuclei are formed during the DSC measurement.

For the first assumption, either the Kissinger (3), Takhor (4) and Augis-Bennett (5) (KTAB) equations can be applied, respectively, given as follows

$$\ln(Q/T_p^2) = -E/RT_P + A \tag{3}$$

$$\frac{d[\ln Q]}{d[1/T_p]} = \frac{E}{R} \tag{4}$$

$$\frac{d[\ln(Q/(T_p - T_0))]}{d[1/T_p]} = \frac{E}{R} \tag{5}$$

where T_p is the temperature of the maximum of the crystallization peak, Q is the heating rate, T_0 is the initial temperature, R is the gas constant, E is the activation energy of the overall crystallization process, including nucleation and crystal growth phenomena, and A is a constant. The plots obtained using the above relations are shown in Fig. 6(a).

The Matusita Eq. (6) may be applied for the second scenario, where further nuclei are formed during the DSC measurement:

$$\ln(Q^n/T_P^2) = -mE/RT_P + A \tag{6}$$

where m represents the dimensionality of crystal growth and determines which equation is correct in each case: If $m = n$, crystallization occurs at a fixed number of nuclei and the KTAB equations are appropriate, whereas if $m = n-1$, nucleation occurs during heating and the Matusita relation is preferable.

In the present study, E/n was first obtained from the Marseglia Eq. (7):

$$\ln(Q/T_P) = -(E/nRT_P) \tag{7}$$

Table IV. Avrami Exponents Obtained from Eq. (2)

T (°C)	745	750	755	760
n	1.2 ± 0.1	1.0 ± 0.2	1.1 ± 0.1	1.4 ± 0.1

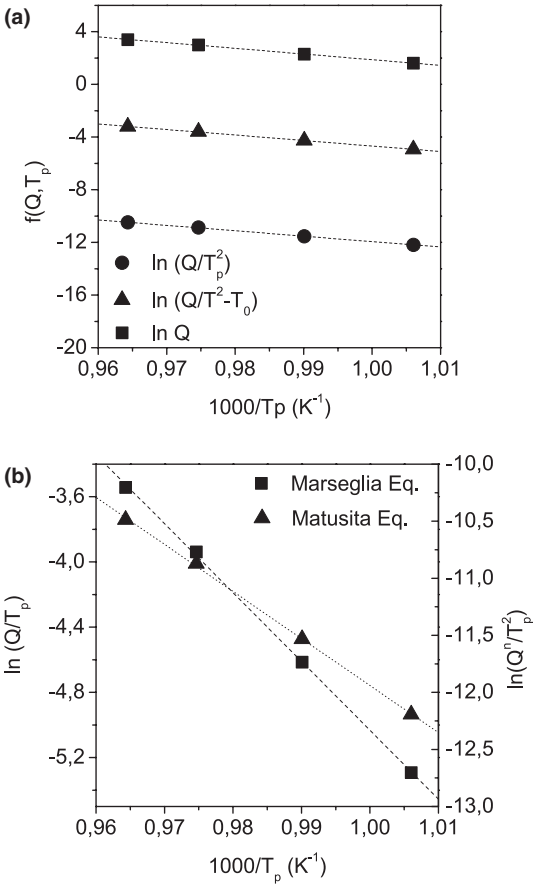

Fig. 6. (a) Kissinger (●), Takhor (■)and Augis-Bennett (▲) plots constructed from the DSC data; (b) Marseglia plot. Q is the heating rate and TP is the DSC crystallization peak.

The n value from the Ozawa equation allows the activation energy E to be calculated from the Marseglia plot [Fig. 6(b)]. The value of m can then be determined from the Matusita plot [Fig. 6(b)].

Table V summarizes the activation energies obtained from the various relations. Activation energy of 350 kJ/mol is determined from the KTAB equations, which is very close to that obtained from the Marseglia relation. As the value of m (0.98) approaches a value of 1 and $m = n = 1$ then, according to Donald,[31] a bulk crystallization mechanism with a constant number of nuclei may be assumed, i.e., a well-nucleated sample in which with the number of nuclei is independent of the heating rate. Crystal growth occurs in two dimensions at

Table V. Activation Energy Obtained from Eqs (3)–(7)

	Activation energy (kJ/mol)		
Ln Q Takhor	Ln (Q/T_p^2) Kissinger	Ln $[Q/(T_p-T_0)]$ Augis-Bennett	Ln (Q/T_P) Marseglia
359 ± 10	343 ± 11	348 ± 11	351 ± 11

a rate of $\sqrt{T}$ (diffusion controlled). In this type of mechanism, which is the same as that reported for the undoped glass,[15] the use of the Kissinger equation is correct. Chen[8] and Hu[11] both reported a value of 300 kJ/mol for the activation energy of a glass of composition $41.2SiO_2$–$29.4Al_2O_3$–$17.6Na_2CO_3$–$11.8LaF_3$ mol% doped with either 3 mol% YbF_3 or 4 mol% ErF_3. An Avrami parameter of 1 was also reported in these works, confirming the nucleating effect of the added RE ions. In contrast, our results show a delay of the onset of LaF_3 crystallization due to Tm_2O_3 additions.

The activation energy of the Tm-doped glass is slightly higher than that of the undoped analogue (338 kJ/mol,[15]), in accordance with the delayed onset of crystallization in the doped glass.

(D) Viscosity: The viscosity-temperature curve of the Tm^{3+}-doped parent glass is shown in Fig. 7, together with that of the undoped glass reported earlier.[15] The temperature dependence of viscosity of the Tm-doped glass was fitted using empirical Vogel-Fulcher-Tammann (VFT) and Avramov equations following the same procedure as that adopted for the undoped material.[15] According to the VFT equation

$$\log \eta = A_1 + \frac{B_1}{T - C_1} \tag{8}$$

the parameters were fitted as $A_1 = -2.7 \pm 0.1$, $B_1 = 6760 \pm 300$, and $C_1 = -190 \pm 50$ (dPa s, K). On employing the Avramov equation

$$\log \eta = A_2 + B_2\left(\frac{T_g}{T}\right)^{C_2} \tag{9}$$

the fitted parameters were $A_2 = -1.0 \pm 0.7$, $B_2 = 8.1 \pm 0.8$, and $C_2 = 1.6 \pm 0.2$ (dPa s, K).

The Tm-doped glass exhibits a lower viscosity than that of the undoped glass over almost the whole studied temperature range (Fig. 7), except around the T_g point, as indicated by the higher value of T_g in the doped glass. Sroda[23] reported a decrease and increase in viscosity at high and low temperatures, respectively, with the addition of some lanthanides in LaF_3-containing glasses, similar to the behavior observed in this study (Fig. 7). At the temperature employed to obtain the glass–ceramics, 620°C, the viscosity of the Tm-doped glass is approximately twice that of the undoped glass (log η = 12.9 and 12.6, respectively), which has important consequences for the crystallization kinetics.

(E) Raman Scattering Spectroscopy: The Raman spectra of the Tm-doped glass and glass–ceramic obtained at 620°C during 40 h are shown in Fig. 8. The spectrum presents a main band at around 480 cm^{-1}, and a very weak signal at 570 cm^{-1}, corresponding to Si–O–Si and Si–O–Al bonds, respectively.[32] Raman bands at 463 and 457 cm^{-1} have been attributed by Gusowski *et al.*[33] to the Ln–F (where Ln = Gd or Y) symmetric stretching vibration; it is likely, therefore, that the corresponding bands in the studied material correspond to La/Tm–F environments, as confirmed by earlier ^{19}F-NMR results for the undoped composition.[14] The band at 720 cm^{-1} can be ascribed to the convolution of the bending mode of the silicate network (775 cm^{-1}) and the Al–O stretching vibration of AlO_4 tetrahedra (700 cm^{-1}).[33] A strong band around 1000 cm^{-1} is observed, corresponding to an asymmetric Si–O stretching vibration mode, in which the contribution of different bands pertaining to different SiO_4 units (denoted as Q^n, where n is the number of bridging oxygens) are included.[33] In addition, two very weak bands at 224 and 317 cm^{-1} can be observed in the glass.

The Tm-doped glass–ceramic exhibits very similar Raman spectra to the parent glass with the main difference being the presence of four sharper resolved bands at 235, 288, 356, and 382 cm^{-1}. Similar peaks in the 200–400 cm^{-1} range were reported by Sroda *et al.*[34] in the Raman spectrum of pure LaF_3 (centered at 289 383, 362, 307 cm^{-1}) and are, thus, ascribable to LaF_3 crystallization in the glass–ceramic. The weak bands at 224 and 317 cm^{-1} observed in the Raman spectrum of the glass could, therefore, be attributed to precursor nuclei of these crystals, since as shown in Fig. 4(c), the parent glass is phase-separated in La-enriched droplets.

(2) Optical Characterization

(A) 1 mol% Tm_2O_3-Doped Glass and Glass–Ceramic: (a) Absorption Spectroscopy: Figure 9 shows the absorption spectra of 1 mol% Tm_2O_3-doped glass and that of the glass–ceramic obtained at 620°C during 40 h. The lower transmittance in the glass–ceramic compared with the glass provides evidence of the influence of crystallinity. Five main bands appear, centered at 1670, 1210, 790, 684 and 470 nm, which can be associated with transitions from the fundamental $^3H_6$ state of Tm^{3+} ions to the $^3F_4$, $^3H_5$ $^3H_4$, $^3F_{2,3}$, and $^1G_4$ excited states, respectively. No appreciable differences between the bands of the glass and glass–ceramic spectra can be observed. This can be due to both the low crystallinity of the samples (6.3 wt%) and the broad

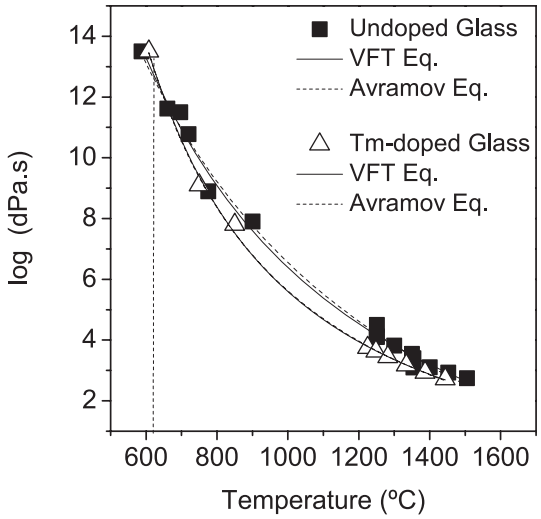

Fig. 7. Viscosity–temperature curves of the undoped glass taken from ref. [15] and the 1 mol% Tm_2O_3-doped glass. Temperature of treatment, 620°C, is indicated with a vertical dashed line.

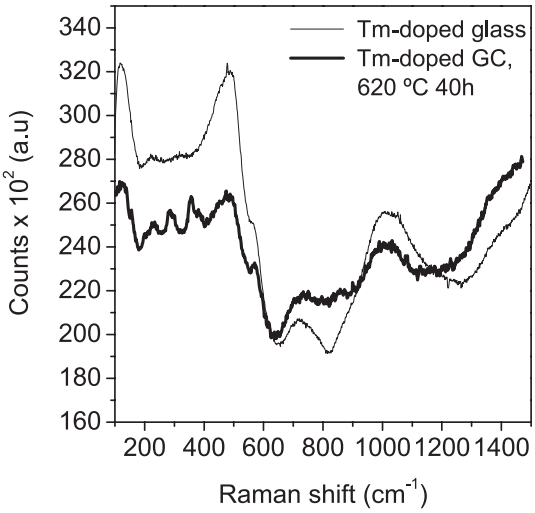

Fig. 8. Raman spectra of the 1 mol% Tm_2O_3-doped glass and glass–ceramic recorded at 532 nm excitation; the band at 115 cm^{-1} is due to the Edge Filter.

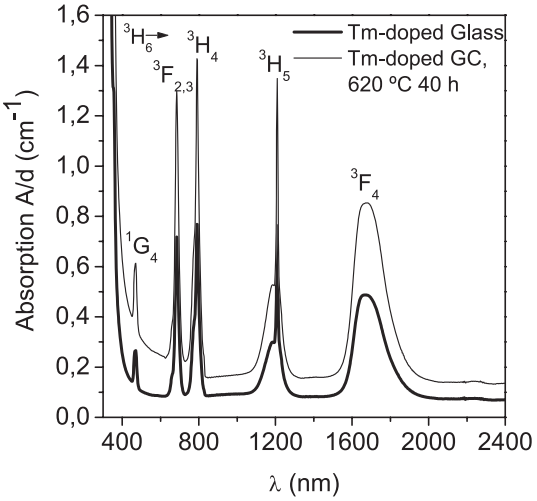

Fig. 9. Absorbance spectra of 1 mol% Tm_2O_3-doped glass and glass–ceramic.

absorption bands of Tm^{3+} ions in glassy environments, which mask their presence in fluoride nanocrystals at room temperature. The same behavior has previously been reported,[35] for Tm^{3+}-doped $NaLaF_4$ glass–ceramics.

(b) Emission Spectra Under Excitation at 488 nm: Figure 10 shows the emission spectra of the glass and glass–ceramic under excitation at 488 nm. It can be seen that there are five main bands common to both glass and glass–ceramic samples centered around 800, 720, 670, 650, and 607 nm, which are associated with the $^3H_4 \rightarrow {}^3H_6$, $^1G_4 \rightarrow {}^3H_5$, $^3F_{2,3} \rightarrow {}^3H_6$, $^1D_2 \rightarrow {}^3H_4$, and $^1G_4 \rightarrow {}^3F_4$ optical transitions, respectively. These bands show a rather broad spectral bandwidth resulting from the amorphous oxygen environments of the Tm^{3+} ions in the glass. Additionally, the presence of sharp and better resolved extra peaks located at 607 and 720 nm can be observed in the glass–ceramic sample (see inset of Fig. 10). These optical transitions are attributed to fluoride crystalline environments of Tm^{3+} and provide evidence for the formation of Tm^{3+}:LaF_3 nano-crystals, similar to those reported previously for Tm^{3+}:$NaLaF_4$ glass–ceramics.[36]

(c) Up-Conversion Spectra Under Excitation at 790 nm: When glass and glass–ceramic samples are excited at 790 nm at room temperature with a pulsed laser, blue emission is observed. Figure 11 shows the up-conversion spectra, in which a main peak appears in both materials from 425 to 500 nm, which is constituted by two contributions at 447 and 477 nm, corresponding to $^1D_2 \rightarrow {}^3F_4$ and $^1G_4 \rightarrow {}^3H_6$ transitions, respectively. These transitions exhibit slightly higher intensity in the glass–ceramic than in the glass, indicating a more efficient process in the glass–ceramic, with respect to that of the glass. In addition, small bands centered at 507 and 537 nm appear which are ascribable to the $^1D_2 \rightarrow {}^3H_5$ transition.

The variation in the emission intensities as a function of the 790 nm laser pumping power was measured in the glass and in the glass–ceramic; the double logarithmic plot of both variables is shown in the inset of Fig. 11. Both slopes are 1.7, approaching a value of 2, indicating a two-photon process, in agreement with previous works.[36] Oomen[37] reported a Tm quenching concentration of the up-conversion process in fluorozirconate glasses, and this effect may contribute to reducing the slope from 2.

Figure 12 represents the energy-level diagram of Tm^{3+}, in which the up-conversion mechanism is indicated. At the 790 nm excitation, the emissor level $^1G_4$ is populated through an excited-state absorption of level $^1H_5$, emitting at 477 nm, while the population of emissor level $^1D_2$ goes through a cross-relaxation process between $^3H_5$ and $^1G_4$ levels, emitting at 447 nm.

(B) Eu_2O_3-Doped Glass and Glass–Ceramic: As was previously mentioned, a Eu_2O_3-doped glass and the corresponding glass–ceramic were synthesized (0.5 mol% Eu_2O_3) to examine the location of lanthanide ions in the LaF_3 nanocrystals. The T_g of this glass, 580°C, is much lower than that of the 1 mol% Tm_2O_3-doped glass, and very similar to that of the undoped glass. Sroda[25] reported that the T_g is not strongly affected by low concentrations of RE ions, in this case 0.5 mol% Eu_2O_3. The Eu_2O_3-doped glass–ceramic was obtained by heat treatment of the parent glass at 620°C during 40 h and crystallization of LaF_3 was confirmed by XRD.

Figures 13(a) and (b) show transmission electron micrographs of the Eu^{3+}-doped glass and glass–ceramic obtained at 620°C during 40 h, respectively. The glass presents La-enriched, phase-separation droplets, around 25 nm in diameter [Fig. 13(a)]. The micrograph of the glass–ceramic [Fig. 13(b)] shows LaF_3 nanocrystals around 20 nm with a homogeneous distribution and a similar crystalline fraction to that of the Tm-doped glass–ceramic.

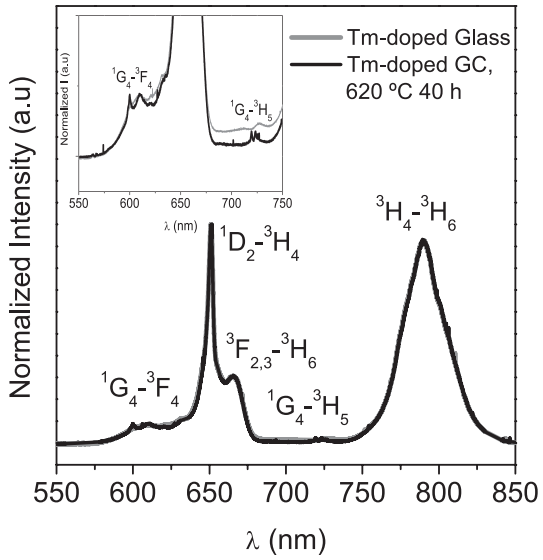

Fig. 10. Emission spectra of 1 mol% Tm_2O_3-doped glass and glass–ceramic under 488 nm excitation.

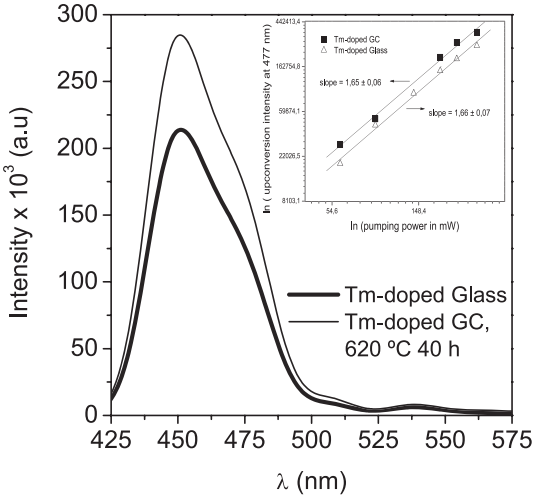

Fig. 11. Up-conversion spectra of 1 mol% Tm_2O_3-doped glass and glass-ceramic under excitation at 790 nm employing a pumping power of 290 mW. The double logarithm plot of the intensity as a function of the pumping power is shown in the inset.

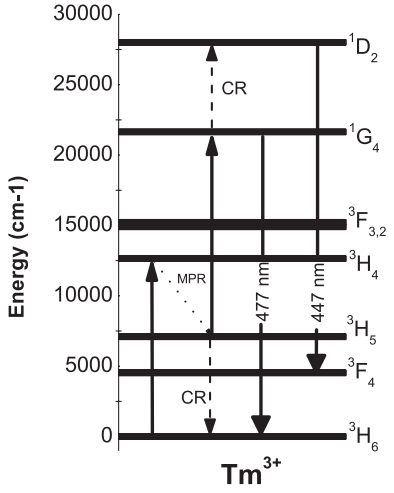

Fig. 12. Tm^{3+} energy-level diagram showing the up-conversion mechanism. (MPR: Multiphonon relaxation, CR:Cross-relaxation)

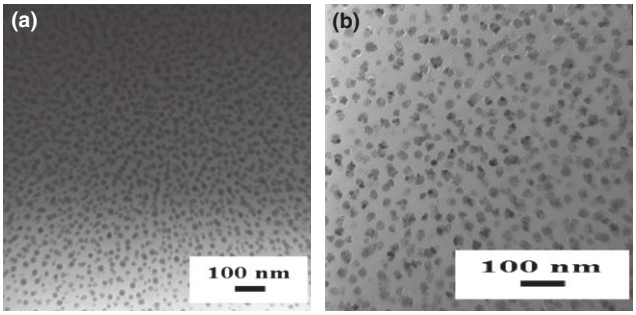

Fig. 13. TEM image of 0.5 mol% Eu_2O_3-doped glass (a) and glass–ceramic (b)

Absorbance spectra of the 0.5 mol% Eu_2O_3-doped glass and glass–ceramic are shown in Fig. 14. The absorption peaks are assigned to the transitions from the ground level $^7F_0$ to the excited levels of Eu^{3+} ions. The strongest absorption peak ($^7F_0 \rightarrow {}^5L_6$ transition) is located at 393 nm. The absorption edge in the glass is shifted to much higher wavelengths compared with the glass–ceramic, and does not show the absorption of the $^5D_4$ and $^5G_2$ levels, which are visible in the glass–ceramic. The fraction of Eu^{3+} ions in the glass is, however, still higher than that in the crystalline environment, which may cause the observed absorption edge shift in the spectrum. The narrower absorption peaks in the glass–ceramic indicate that the Eu^{3+} environment is more crystalline.[38,39]

An Ar laser was employed to record emission spectra of the Eu^{3+}-doped glass and glass–ceramic under excitation at 488 nm (Fig. 15). In general, there are additional and narrower bands in the glass–ceramic compared with the glass, indicating a more crystalline environment of Eu^{3+} in comparison to the glass. The emission bands correspond to the transitions of the excited $^5D_0$ energy level to the ^7F_n levels of Eu^{3+}. The emission intensity of the $^5D_0 \rightarrow {}^7F_2$ transition is electric-dipole allowed (sensitive to the local environment) and the transition $^5D_0 \rightarrow {}^7F_1$ is magnetic dipole allowed (independent of the host matrix). The fluorescence intensity ratio (R) of the $^5D_0 \rightarrow {}^7F_2$ to $^5D_0 \rightarrow {}^7F_1$ transitions is used to establish the degree of asymmetry in the vicinity of the Eu^{3+} ions and the covalence of the Eu–O bonds for various Eu^{3+}-doped systems.[40] The value of R increases with a lowering in symmetry around the Eu^{3+} ions and higher covalence of the Eu–O bonds.[41,42] The Eu^{3+}-doped glass–ceramic presents a ratio of $^5D_0 \rightarrow {}^7F_1$ to $^5D_0 \rightarrow {}^7F_2$ which is slightly higher than that of the doped glass, indicating that the Eu^{3+} environment become more symmetric and that Eu^{3+} is, thus, distributed between both crystalline and amorphous phases. The appearance of the non-degenerate $^5D_0 \rightarrow {}^7F_0$ transition indicates that the Eu^{3+} ion is in an environment of low symmetry,[43] corresponding to Eu^{3+} ions in glassy environments. The magnetic-dipole transition $^5D_0 \rightarrow {}^7F_1$ splits into three components, indicating that the crystallographic sites of the Eu^{3+} ions in the crystalline lattice adopt symmetry as low as orthorhombic, monoclinic or triclinic. The better resolved band at 580 nm could be an indication that the C_2 site symmetry of La^{3+} is partially occupied by Eu^{3+} in the LaF_3 crystals.[43]

Emission spectra of the glass and glass–ceramic were also recorded under excitation at 393 nm and are shown in the inset of Fig. 15. A broad band from 400 to 500 nm appears which could be ascribed to the $4f^6 5d$–$4f^7$ transition of Eu^{2+} ions.[44] The reduction in Eu^{3+} to Eu^{2+} has been reported to occur in fluoride-containing glasses doped with Eu^{3+} in air, and is related with the optical basicity of the host material and with a charge compensation model.[44,45] In oxyfluoride glass–ceramics, the transformation $Eu^{3+} \rightarrow Eu^{2+}$ occurs when part of the Eu^{3+} ions are incorporated into a fluorine-enriched environment, such as the fluoride crystals. Yang *et al.*[44] obtained very similar emission spectra in glasses and

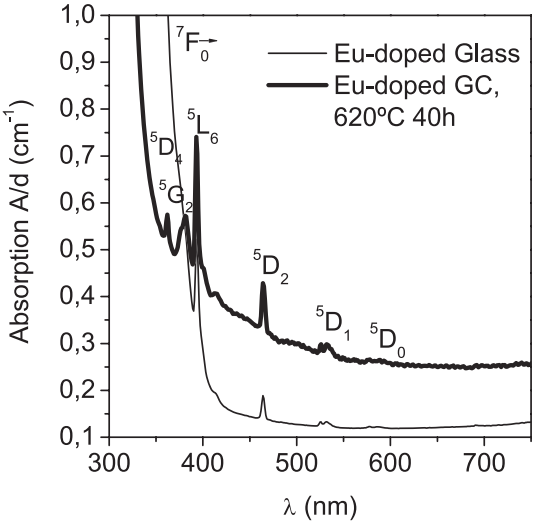

Fig. 14. Absorbance spectra 0.5 mol% Eu_2O_3-doped glass and glass–ceramic

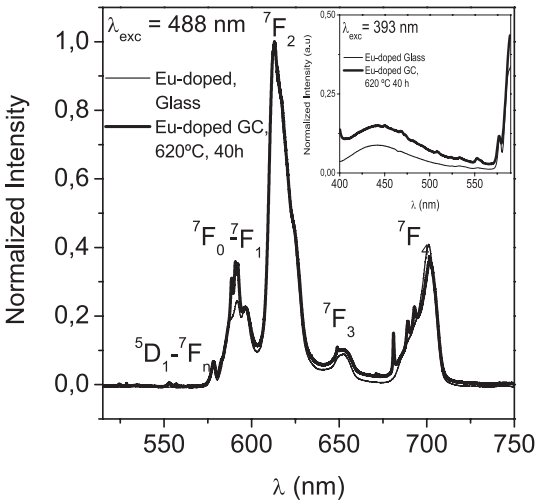

Fig. 15. Emission spectra of 0.5 mol% Eu_2O_3-doped glass and glass–ceramic under 488 nm excitation, and under 393 nm excitation (inset).

glass–ceramics of composition $44SiO_2$–$28Al_2O_3$–17NaF–$11YF_3$–$xEuF_3$ (x = 0.1, 0.2, 0.5, and 0.8) under excitation at 394 nm. Lin *et al.*[46] observed an increase in intensity of the emission broad band in the blue range of Eu^{2+} with increasing fluorine content in CaF_2-oxyfluoride glasses. From the normalized intensity ratio of the broad band centered at around 440 nm shown in the inset of Fig. 15, a higher Eu^{2+}/Eu^{3+} ratio is found in the glass–ceramic with respect to the glass, indicative of the distribution of Eu^{3+} ions in the crystal structure of LaF_3.

The quantification of the RE ions located in the crystalline LaF_3 phase is planned in a future work exploiting different techniques such as absorption[47] and time resolved luminescence measurements.[48,49]

IV. Conclusions

Tm^{3+}-doped glass–ceramics were synthesized, where LaF_3 nanocrystals of 20 nm in diameter are precipitated on heat treatment of the parent glass. The effect of the addition of Tm_2O_3 on LaF_3 crystallization has been studied and compared with that found in the undoped glass. A longer induction time for crystallization of LaF_3 is observed in the Tm^{3+}-doped glass with respect to the undoped analogue. The lower tendency of the Tm-doped glass to crystallize is likely to result from both a slightly higher activation energy for crystallization and a higher viscosity at the temperature of glass–ceramic formation. The addition of Tm^{3+} affects the phase separation in the parent glass, giving rise to some larger crystals in the Tm-doped glass–ceramics. Raman spectra confirm the existence of La–F nuclei in the parent-glass precursors of the LaF_3 nano-crystals, as well as La/Tm–F bonds in the glass and in the glass–ceramics.

Photoluminescence emission measurements indicate that the Tm^{3+} and Eu^{3+} cations are distributed between the glass matrix and the LaF_3 nano-crystals. Moreover, the Eu^{3+} ions are partially reduced to Eu^{2+}, as a consequence of the fluorine-rich environment.

The Tm^{3+} up-conversion spectra involve a two-photon absorption process with a higher blue emission intensity in the glass–ceramic compared with the glass.

Acknowledgments

The authors thank Dr. R. Mercatelli and Dr. F. Quercioli for access to the INO-CNR facilities to perform the up-conversion measurements, Dr. G. Barreto for his assistance at ILL during the neutron-diffraction measurements, Prof. D. Ehr and Dr. A. Herrmann for their collaboration and support with Eu- luminescence study, V.Sreeramulu for his assistance with Raman spectroscopy measurements and Dr. F. Muñoz for his valuable discussions. Financial support from the European Union under INTERCONY project (NMP3-CT-2006-033200), Spanish MICINN under projects MAT2010-20459 and MAT2010-17443 and the Comunidad de Madrid under Grant PHAMA-S2009/MAT-1756 is acknowledged. A. De Pablos-Martín thanks the CSIC for a JAE-predoctoral fellowship.

References

[1]Y. Wang and J. Ohwaki, "New Transparent Vitroceramics Codoped With Er^{3+} and Yb^{3+} for Efficient Frequency Upconversion," *Appl. Phys. Lett.*, **63** [24] 3268–70 (1993).

[2]A. Bensalah, M. Mortier, G. Patriarche, P. Gredin, and D. Vivien, "Synthesis and Optical Characterizations of Undoped and Rare-Earth-Doped CaF_2 Nanoparticles," *J. Solid State Chem.*, **179** [8] 2636–44 (2006).

[3]N. M. Strickland and G. D. Jones, "Site-Selective Spectroscopy of Tm^{3+} Centers in CaF_2:Tm^{3+}," *Phys. Rev. B*, **56** [17] 10916–29 (1997).

[4]J. Zhang, D. He, Z. Duan, L. Zhang, S. Dai, and L. Hu, "Mechanisms and Concentrations Dependence of up-Conversion Luminescence in Tm^{3+}/Yb^{3+} Codoped Oxyfluoride Glass-Ceramics," *Phys. Lett. A*, **337** [4–6] 480–6 (2005).

[5]S. F. León-Luis, J. Abreu-Afonso, J. Peña-Martínez, J. Méndez-Ramos, A. C. Yanes, J. del-Castillo, and V. D. Rodríguez, "Up-Conversion and Colour Tunability in Yb^{3+}–Er^{3+}–Tm^{3+} co-Doped Transparent Nano-Glass-Ceramics," *J. Alloy. Compd.*, **479** [1–2] 557–60 (2009).

[6]F. Zeng, G. Ren, X. Qiu, and Q. Yang, "Effect of Different Er^{3+} Compounds Doping on Microstructure and Photoluminescent Properties of Oxyfluoride Glass Ceramics," *Phys. B*, **403** [13–16] 2417–22 (2008).

[7]N. Hémono, G. Pierre, F. Muñoz, A. de Pablos-Martín, M. J. Pascual, and A. Durán, "Processing of Transparent Glass-Ceramics by Nanocrystallisation of LaF_3," *J. Eur. Ceram. Soc.*, **29** [14] 2915–20 (2009).

[8]D. Chen, Y. Wang, Y. Yu, and E. Ma, "Influence of Yb^{3+} Content on Microstructure and Fluorescence of Oxyfluoride Glass Ceramics Containing LaF_3 Nanocrystals," *Mater. Chem. Phys.*, **101** [2–3] 464–9 (2007).

[9]W. Jin, Q. Xusheng, F. Xianping, and W. Minquan, "Preparation and Luminescence of Er^{3+} Doped Oxyfluoride Glass Ceramics Containing LaF_3 Nanocrystals," *J. Rare Earth*, **24** [1] 67–71 (2006).

[10]E. Ma, Z. Hu, Y. Wang, and F. Bao, "Influence of Structural Evolution on Fluorescence Properties of Transparent Glass Ceramics Containing LaF_3 Nanocrystals," *J. Lumin.*, **118** [2] 131–8 (2006).

[11]Z. Hu, Y. Wang, F. Bao, and W. Luo, "Crystallisation Behaviour and Microstructure Investigations on LaF_3 Containing Oxyfluoride Glass Ceramics," *J. Non-Cryst. Solids*, **351** [8–9] 722–8 (2005).

[12]J. R. Barros, Ch. Bocker, and Chr. Rüssel, "The Effect of Er^{3+} and Sm^{3+} on Phase Separation and Crystallization in Na_2O/K_2O/BaF_2/BaO/Al_2O_3/SiO_2 Glasses," *Solid State Sci.*, **12** [12] 2086–90 (2010).

[13]S. Bhattacharyya, Th. Höche, N. Hemono, M. J. Pascual, and P. A van Aken, "Nanocrystallization in LaF_3-Na_2O-Al_2O_3-SiO_2 Glass," *J. Cryst. Growth*, **311** [18] 4350–5 (2009).

[14]F. Muñoz, A. de Pablos-Martín, N. Hémono, M. J. Pascual, A. Durán, L. Delevoye, and L. Montagne, "NMR Investigation of the Crystallization Mechanism of LaF_3 and $NaLaF_4$ Phases in Aluminosilicate Glasses," *J. Non-Cryst. Solids*, **357** [5] 1463–8 (2011).

[15]A. de Pablos-Martín, N. Hémono, G. C. Mather, S. Bhattacharyya, T. Höche, H. Bornhöft, J. Deubener, F. Muñoz, A. Durán, and M. J. Pascual, "Crystallization Kinetics of LaF_3 Nanocrystals in an Oxyfluoride Glass," *J. Am. Ceram. Soc.*, **94** [8] 2420–8 (2011).

[16]G. Litscher, Z. Xie, L. Wang, and I. Gaischek, "Blue 405 nm Laser Light Mediates Heart Rate—Investigations at the Acupoint Neiguan (Pe.6) in Chinese Adults," *North Am. J. Med. Sci.*, **1** [5] 226–31 (2009).

[17]D. K. Chatterjee, M. K. Gnanasammandhan, and Y. Zhang, "Upconverting Fluorescent Nanoparticles for Biomedical Applications," *Small*, **6** [24] 2781–95 (2010).

[18]X. Qiao, Q. Luo, X. Fan, and M. Wang, "Local Vibration Around Rare Earth Ions in Alkaline Earth Fluorosilicate Transparent Glass and Glass Ceramics Using Eu^{3+} Probe," *J. Rare Earth*, **26** [6] 883–8 (2008).

[19]J. Rodriguez-Carvajal, "Recent Advances in Magnetic Structure Determination by Neutron Powder Diffraction," *Phys. B*, **192** [1–2] 55–69 (1993).

[20]T. Höche, J. W. Gerlach, and T. Petsch, "Static-Charging Mitigation and Contamination Avoidance by Selective Carbon Coating of TEM Samples," *Ultramicroscopy*, **106** [11–12] 981–5 (2006).

[21]M. J. Pascual, L. Pascual, and A. Durán, "Determination of Viscosity-Temperature Curve for Glasses, on the Basis of Fixed Viscosity Points Determined by Heating Microscopy," *Phys. Chem. Glasses*, **42** [1] 61–6 (2001).

[22]M. J. Pascual, A. Durán, and M. O. Prado, "A new Method for Determining Fixed Viscosity Points of Glasses," *Phys. Chem. Glasses*, **46** [5] 512–20 (2005).

[23]M. Sroda, "Effect of Er_2O_3 on Thermal Stability of Oxyfluoride Glass," *J. Therm. Anal. Calorim.*, **97** [1] 239–43 (2009).

[24]C. Rüssel, "Nanocrystallization of CaF_2 From Na_2O/K_2O/CaO/CaF_2/Al_2O_3/SiO_2 Glasses," *Chem. Mater.*, **17** [23] 5843–7 (2005).

[25]A. Zalkin and D. H. Templeton, "Refinement of the Trigonal Crystal Structure of Lanthanum Trifluoride With Neutron Diffraction Data," *Acta Cryst. B*, **41** [2] 91–3 (1985).

[26]W. L. Bragg, "Crystal Structure," *Nature*, **105** [2646] 646–8 (1920).

[27]L. B. McCusker, R. B. von Dreele, D. E. Cox, D. Louër, and P. Scardi, "Rietveld Refinement Guidelines," *J. Appl. Cryst*, **32** [1] 36–50 (1999).

[28]X. Orlhac, C. Fillet, P. Deniard, A. M. Dulac, and R. Brec, "Determination of the Crystallized Fractions of a Largely Amorphous Multiphase Material by the Rietveld Method," *J. Appl. Cryst*, **34** [2] 114–118 (2001).

[29]A. de Pablos-Martín, G. C. Mather, F. Muñoz, S. Bhattacharyya, Th. Höche, J. R. Jinschek, T. Heil, A. Durán, and M. J. Pascual, "Design of oxy-Fluoride Glass-Ceramics Containing $NaLaF_4$ Nano-Crystals," *J. Non-Cryst. Solids*, **356** [52–54] 3071–9 (2010).

[30]M. J. Pascual, C. Lara, and A. Durán, "Non-Isothermal Crystallisation Kinetics of Devitrifiying RO-BaO-SiO_2 (R = Mg, Zn) Glasses," *Phys. Chem. Glasses: Eur. J. Glass Sci. Technol., Part B*, **47** [5] 572–81 (2006).

[31]I. W. Donald, "Crystallisation Kinetics of a Lithium Zinc Silicate Glass Studied by DTA and DSC," *J. Non-Cryst. Solids*, **345–346**, 120–6 (2004).

[32]K. Chah, B. Boizot, B. Reynard, D. Ghaleb, and G. Petite, "Micro-Raman and EPR Studies of b-Radiation Damages in Aluminosilicate Glass," *Nucl. Instr. Meth. B*, **191** [1–4] 337–41 (2002).

[33]M. A. Gusowski, A. Gagor, M. Trzebiatowska-Gusowska, and W. Ryba-Romanowski, "Crystal Structure and Vibrational Properties of new Luminescent Hosts K_3YF_6 and K_3GdF_6," *J. Solid State Chem.*, **179** [10] 3145–50 (2006).

[34]M. Sroda, C. Paluszkiewicz, M. Reben, and B. Handke, "Spectroscopic Study of Nanocrystallization of Oxyfluoride Glasses," *J. Mol. Struct.*, **744–747**, 647–51 (2005).

[35]A. de Pablos-Martín, M. O. Ramírez, A. Durán, L. E. Bausá, and M. J. Pascual, "Tm^{3+} Doped oxy-Fluoride Glass-Ceramics Containing $NaLaF_4$ Nano-Crystals," *Opt. Mater.*, **33** [2] 180–5 (2010).

[36]F. Song, L. Han, C. Zou, J. Su, K. Zhang, L. Yan, and J. Tian, "Upconversion Blue Emission Dependence on the Pump Mechanism for Tm^{3+}-Heavy-Doped $NaY(WO_4)_2$ Crystal," *Appl. Phys. B*, **86** [4] 653–60 (2007).

[37]E. W. J. L. Oomen, "Up-Conversion of red Light Into Blue Light in Thulium Doped Fluorozirconate Glasses," *J. Lumin.*, **50** [6] 317–32 (1992).

[38]L. A. Bueno, A. S. Gouveia-Neto, E. B. da Costa, Y. Messaddeq, and S. J. L. Ribeiro, "Structural and Spectroscopic Study of Oxyfluoride Glasses and Glass-Ceramics Using Europium ion as a Structural Probe," *J. Phys.: Condens. Matter*., **20** [14] 145201–7 (2008).

[39]Y. Dwivedi and S. B. Rai, "Optical Properties of Eu^{3+} in Oxyfluoroborate Glass and its Nanocrystalline Glass," *Opt. Mater*., **31** [1] 87–93 (2008).

[40]P. Babu and C. K. Jayasankar, "Optical Spectroscopy of Eu^{3+} Ions in Lithium Borate and Lithium Fluoroborate Glasses," *Phys. B*, **279** [4] 262–81 (2000).

[41]R. Reisfeld, E. Zigansky, and M. Gaft, "Europium Probe for Estimation of Site Symmetry in Glass Films, Glasses and Crystals," *Mol. Phys*., **102** [11–12] 1319–30 (2004).

[42]K. Binnemans, K. Van Herck, and C. Gorller-Walrand, "Influence of Dipicolinate Ligands on the Spectroscopic Properties of Europium (III) in Solution," *Chem. Phys. Lett*., **266** [3–4] 297–302 (1997).

[43]X. Zhang, T. Hayakawa, and M. Nogami, "Size-Dependence of LaF_3:Eu^{3+} Nanocrystals on Eu^{3+} Photoluminescence Intensity," *IOP Conf. Ser.: Mater. Sci. Eng*., **1**, 012021, 7 pp (2009).

[44]F. Yang, G. Chen, Z. You, C. Sun, J. Cao, Y. Ji, Y. Wang, Y. Wang, Z. Zhu, J. Li, and C. Tu, "The Transformation of $Eu^{3+} \rightarrow Eu^{2+}$ in SiO_2–Al_2O_3–NaF–YF_3: Eu Glasses and Glass Ceramics," *Mater. Lett*., **65** [9] 1337–9 (2011).

[45]S. Liu, G. Zhao, W. Ruan, Z. Yao, T. Xie, J. J. Hao, Y. J. Wang, and G. Han, "Reduction of Eu^{3+} to Eu^{2+} in Aluminoborosilicate Glasses Prepared in Air," *J. Am. Ceram. Soc*., **91** [8] 2740–2 (2008).

[46]Z. Lin, H. Zeng, Y. Yang, X. Liang, and G. Chen, "The Effect of Fluorine Anions on the Luminescent Properties of Eu-Doped Oxyfluoride Aluminosilicate Glasses," *J. Am. Ceram. Soc*., **93** [10] 3095–8 (2010).

[47]M. Mattarelli, M. Montagna, E. Moser, A. Chiasera, V. Tikhomirov, A. B. Seddon, S. Chaussedent, G. Nunzi Conti, S. Pelli, G. C. Righini, L. Zampedri, and M. Ferrari, "Tm^{3+}-Activated Transparent oxy-Fluoride Glass Ceramics: Structural and Spectroscopic Properties," *J. Non-Cryst. Solids*, **345–346**, 354–8 (2004).

[48]O. Péron, B. Boulard, Y. Jestin, M. Ferrari, C. Duverger-Arfuso, S. Kodjikian, and Y. Gao, "Erbium Doped Fluoride Glass-Ceramics Waveguides Fabricated by PVD," *J. Non-Cryst. Solids*, **354** [30] 3586–91 (2008).

[49]B. Boulard, G. Alombert, I. Savelii, C. Duverger-Arfuso, Y. Gao, M. Ferrari, and F. Prudenzano, "Er^{3+}/Yb^{3+}/Ce^{3+} co-Doped Fluoride Glass Ceramics Waveguides for Application in the 1.5 μm Telecommunication Window," *Adv. Sci. Technol*., **71**, 16–21 (2010). □